Journal of Power Sources 201 (2012) 274–279

Contents lists available at SciVerse ScienceDirect

Journal of Power Sources

journal homepage: www.elsevier.com/locate/jpowsour

Synthesis and characterization of $LiFePO_4$ and $LiFePO_4$/C cathode material from lithium carboxylic acid and Fe^{3+}

Kerun Yang[a,b], Zhenghua Deng[a,b,c,*], Jishuan Suo[a,b]

[a] Chengdu Institute of Organic Chemistry, Chinese Academy of Sciences, Chengdu, Sichuan 610041, PR China
[b] Graduate School of Chinese Academy of Sciences, Beijing 100039, PR China
[c] Zhongke Laifang Power Science & Technology Co., Ltd, Chengdu, Sichuan 610041, PR China

ARTICLE INFO

Article history:
Received 25 May 2011
Received in revised form 5 November 2011
Accepted 7 November 2011
Available online 15 November 2011

Keywords:
Lithium iron phosphate
Lithium carboxylic acid
Reductive mechanism

ABSTRACT

Olivine $LiFePO_4$ and $LiFePO_4$/C are successfully prepared by a simple solid-state reaction using $FePO_4{\cdot}2H_2O$, lithium oxalate and glucose (bare $LiFePO_4$ without adding glucose) as raw materials. The structure of the $LiFePO_4$ and $LiFePO_4$/C is investigated by X-ray diffraction (XRD). The micromorphology of $LiFePO_4$ and $LiFePO_4$/C is observed using scanning electron microscopy (SEM) and BET, and the in situ coating of carbon on the particles is observed by transmission electron microscopy (TEM) and Raman spectrum. Furthermore, the electrochemical properties are evaluated by cyclic voltammograms (CVs), electrochemical impedance spectra (EIS) and constant current charge/discharge cycling tests. The results show that carbon coated $LiFePO_4$ can deliver better battery performance than the bare $LiFePO_4$. It exhibits initial discharge capacities of 162, 142 and 112 mA h g^{-1} at rates of 0.1, 1 and 10 C, respectively, and it presents excellent capacity retention as there is tiny capacity fade after 100 cycles. Moreover, the reductive mechanism of using lithium carboxylic acid to synthesize $LiFePO_4$ is firstly mentioned.

1. Introduction

Lithium iron phosphate ($LiFePO_4$) has been considered one of the most promising cathode materials for use in the electric and hybrid electric vehicles [1,2] because of its high theoretical capacity (170 mA h g^{-1}), high safety, environmental benignity, flat discharge voltage, and low cost [3–10]. However, there are two major impediments to the commercial application of $LiFePO_4$: one is the low electronic conductivity (10^{-7}–10^{-9} S cm^{-1}), which leads to its poor rate capability; the other is the slow lithium-ion diffusion across the $LiFePO_4$|$FePO_4$ boundary [3,11]. To eliminate the two major impediments of $LiFePO_4$, numerous approaches such as conductive additive coating [12–14], supervalence cation doping [15,16], and minimizing particle size by different synthesis routes [17–19], have been reported. The synthesis method has been an important factor for its large-scale commercial manufacture. Various synthesis routes have been proposed to prepare $LiFePO_4$, such as solid-state reaction [20–23], sol–gel technique [24], molten salt synthesis [25], coprecipitation method [26], hydrothermal synthesis [27,28], microwave heating [29], mechanical activation [30–35] and so on. Compared to other methods, solid-state reaction route can meet the needs of large-scale commercial manufacture [36]. However, FeC_2O_4, Li_2CO_3 or LiOH, $NH_4H_2PO_4$, were usually selected as starting materials to synthesize $LiFePO_4$. Apart from being low productivity and involving evolution of unfavorable gas, several phase reaction and using volatile organic solvents to protect Fe^{2+} are not considered commercially favorable.

In this study, lithium oxalate ($Li_2C_2O_4$), $FePO_4{\cdot}2H_2O$ and glucose were used as raw materials to prepare $LiFePO_4$/C composite. Herein, $Li_2C_2O_4$ was introduced as lithium source, and $FePO_4{\cdot}2H_2O$ was proposed to be both the iron and phosphorus source. It is favorable to mix well, react completely and get homogeneous $LiFePO_4$/C samples because the decrease of reaction phase. At the same time, this method using $FePO_4{\cdot}2H_2O$ as the starting material are environmental benignity and high productivity for the production of $LiFePO_4$ material, compared with divalent iron starting materials such as $FeC_2O_4{\cdot}2H_2O$ and $NH_4H_2PO_4$, which generate CO_2 and NH_3. Furthermore, the reductive mechanism of using $Li_2C_2O_4$ to synthesize bare $LiFePO_4$ is firstly mentioned.

2. Experimental

2.1. Synthesis of the $LiFePO_4$ and $LiFePO_4$/C

$FePO_4{\cdot}2H_2O$, $Li_2C_2O_4$ and glucose were dissolved in de-ionized water, and then the above solution was thoroughly mixed by ball-milling in a planetary QM-3SP2 mill for 6 h. The homogeneous

* Corresponding author at: Chengdu Institute of Organic Chemistry, Chinese Academy of Sciences, No. 9 Section 4, Renmin Nan lu, Chengdu, Sichuan 610041, China. Tel.: +86 28 85229252; fax: +86 28 85233426.
E-mail address: zhdeng@cioc.ac.cn (Z. Deng).

0378-7753/$ – see front matter © 2011 Elsevier B.V. All rights reserved.
doi:10.1016/j.jpowsour.2011.11.019

slurry was dried at 120 °C for 6 h to obtain the precursor. The powder was synthesized in two steps: the precursors were first decomposed at 500 °C for 2 h, and then sintered at 700 °C for 15 h. Decomposing and sintering were both carried out in a flowing N_2 atmosphere. Bare LiFePO4 was synthesized without using glucose.

2.2. Characterization of the $LiFePO_4$ and $LiFePO_4$/C

Resonant Raman scattering spectra were recorded at room temperature with a Invia Raman Microscope in a backscattering configuration, with an excitation wavelength of 325 nm. X-ray powder diffraction (XRD) of the powders was carried out on a Philips X' Pert diffractometer equipped with Cu-$K\alpha$ radiation of $\lambda = 0.15418$ nm in the range of $15° < 2\theta < 80°$. The micromorphology of the precursor, $LiFePO_4$ and $LiFePO_4$/C was observed using a Impect F (FEI Company) scanning electron microscopy. More detailed analysis of the $LiFePO_4$/C microstructure was accomplished using Hitachi H-600 transmission electron microscopy. The specific surface area of the samples was detected by nitrogen adsorption/desorption at −196 °C using a Builder SSA-4200 apparatus, and carbon content was obtained from a CARLO ERBA 1106 elemental analyzer (Italy).

2.3. Electrochemical measurements

Electrochemical measurements of the $LiFePO_4$ and $LiFePO_4$/C composite were accomplished by assembling CR2032 coin cells. The electrode was made by dispersing the $LiFePO_4$/C (or $LiFePO_4$), super-p carbon black and an aqueous binder LA132 (from Indigo, China) homogeneously (using de-ionized water as solvent) in a weight ratio of 80:10:10, casting the mixture uniformly onto an aluminum foil and drying at 100 °C. All electrodes were punched in the form of a disk with a diameter of 14.5 mm (area of 1.65 cm^2), pressed, dried at 100 °C under vacuum for 8 h, and then weighed to determine the active mass. A typical electrode disk contained 3–5 mg cm^{-2} of $LiFePO_4$/C (or $LiFePO_4$) active material with a thickness of 300–400 μm when coated on aluminum foil. The electrochemical performance of the $LiFePO_4$/C (or $LiFePO_4$) was evaluated with lithium metal foil as the counter electrode and Celguard 2400 as the separator. The cell assembly was carried out in an argon-filled dry box. The electrolyte used was a 1 mol L^{-1} $LiPF_6$ solution in a mixture of ethylene carbonate, dimethyl carbonate and ethylene methyl carbonate (1:1:1 by volume). The cell cycled through a constant current charge and discharge between 2.5 and 4.3 V (vs. Li/Li^+) using a Neware Battery Tester (China). Cyclic voltammetry measurements were performed using an Arbin Instrument (USA) at a scan rate of 0.1 mV s^{-1} between 2.5 and 4.3 V. Electrochemical impedance spectra were measured by using a Solatron 1260 Impedance Analyzer in the frequency range from 0.1 Hz to 10^6 Hz at the open circuit with an AC voltage signal of 5 mV. All the tests were performed at room temperature.

3. Results and discussion

Fig. 1 shows the SEM images of the precursors. It can be observed that the size distribution in Fig. 1(b) was better than that in Fig. 1(a), indicating that glucose may be in favor of improving the dispersion degree of the precursor.

The X-ray diffraction patterns of $LiFePO_4$ and $LiFePO_4$/C are shown in Fig. 2. As can be seen form Fig. 2, no impurities are detected in sample $LiFePO_4$/C, suggesting that the carbon derived from glucose can effectively avoid the appearance of the impurity phase during the heat-treatment. And there is no obvious diffraction response of the carbon because of its low content or amorphous state. The results obtained from elemental analysis show that the amount of carbon in the $LiFePO_4$/C composite is 3.85 wt%. In sample

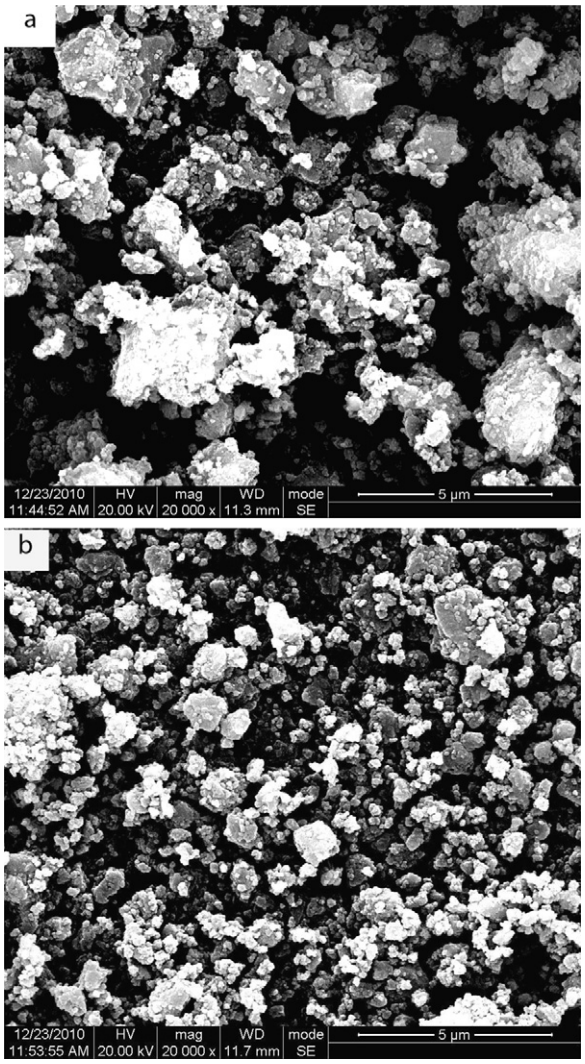

Fig. 1. SEM images of the precursors: (a) without adding glucose, (b) adding glucose.

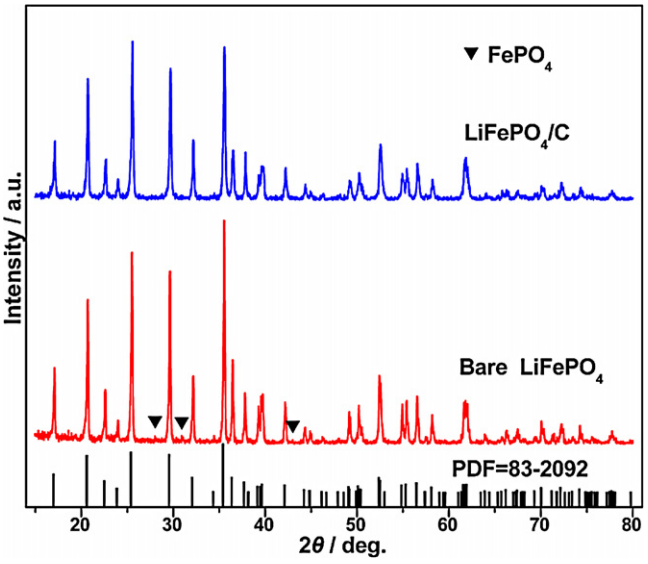

Fig. 2. XRD patterns of bare $LiFePO_4$ and $LiFePO_4$/C.

Table 1
The lattice parameters and calculated crystallite size of the $LiFePO_4$ and $LiFePO_4$/C.

Sample ID	a (Å)	b (Å)	c (Å)	Cell volume (Å^3)	Crystallite size, D (nm)
$LiFePO_4$	10.344	6.018	4.700	292.6	32
$LiFePO_4$/C	10.328	6.008	4.697	291.9	25
PDF=83-2092	10.334	6.01	4.693	291.5	

$LiFePO_4$, an impure phase is detected, which may be attributable to $FePO_4$, indicating that $FePO_4$ does not entirely convert to $LiFePO_4$ during the heat-treatment. As we know, the dispersion degree of reactants has an enormous effect on solid-phase reaction, and a good uniformity in size distribution can be propitious to the completeness of solid-phase reaction. But as can be seen from Fig. 1(a), the precursor of the sample $LiFePO_4$ has an inhomogeneous size distribution which may be result to incompleteness of the solid-phase reaction. At the same time, the additional reductant was not added in this reaction. Hence, the reason for the appearance of the impure phase in the sample $LiFePO_4$ could be in connection with the incompleteness of the reductive reaction.

The lattice constants, the cell volume and crystallite size of $LiFePO_4$ and $LiFePO_4$/C are listed in Table 1. It shows that the lattice constants of $LiFePO_4$ and $LiFePO_4$/C are approximately similar, indicating that the addition of glucose as carbon source had no obvious effect on the crystal structure of $LiFePO_4$ itself. However, the crystallite sizes are 32 nm for pure $LiFePO_4$ and 25 nm for $LiFePO_4$/C composite, respectively. It is believed that the small particle size is useful for the intercalation/de-intercalation process of lithium ions.

From Fig. 2, it can also be seen that olivine structure with an orthorhombic Pnma space group is the main crystalline phase in the sample $LiFePO_4$. But only $FePO_4$ and $Li_2C_2O_4$ were used to synthesize $LiFePO_4$, and no additional reductant was added. So the reactions may be according to the following mechanism:

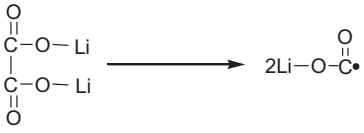

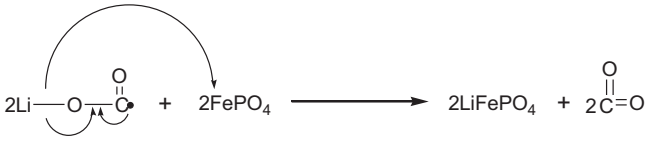

The C–C bond which is the weakest bond in $Li_2C_2O_4$ was firstly broken to form free radical, after that the reductive reaction between free radical and $FePO_4$ immediately happened to generate $LiFePO_4$ and carbon dioxide. Because free radicals cannot exist stably, the above reactions almost simultaneously occur. The further investigations about the reactions are under way.

Fig. 3 shows the SEM images of $LiFePO_4$ and $LiFePO_4$/C. It can be seen from Fig. 3 that the particle size of $LiFePO_4$/C is smaller than bare $LiFePO_4$, indicating that $LiFePO_4$/C has a lower degree of crystallization. The reason for this could be that the carbon derived from glucose can effectively inhibit the growth of the particle, which is corresponding with the XRD patterns. There is considerable nano-sized microstructure on the surface of the sample $LiFePO_4$/C, however, sample $LiFePO_4$ shows a glossy surface. The glossy surface of the powders and the increase in particle size can also be attributed to the higher crystallization degree of the sample. The data from the BET measurement shown in Table 2, give a specific surface area of 1.05 $m^2\,g^{-1}$ and 29.86 $m^2\,g^{-1}$ for the bare $LiFePO_4$ and the $LiFePO_4$/C, respectively. The $LiFePO_4$/C composite shows the larger specific surface area, which is in good agreement with Fig. 3.

Table 2
The specific surface area of the $LiFePO_4$ and $LiFePO_4$/C.

Sample ID	Specific surface area ($m^2\,g^{-1}$)
$LiFePO_4$	1.05
$LiFePO_4$/C	29.86

To confirm how the carbon is distributed within the $LiFePO_4$ powder, the $LiFePO_4$/C powders were observed under TEM as shown in Fig. 4. There is a discrete carbon layer coating on the surface of the $LiFePO_4$ particles. The connection between $LiFePO_4$ and carbon is tight, which is profitable to the improvement of electric conductivity.

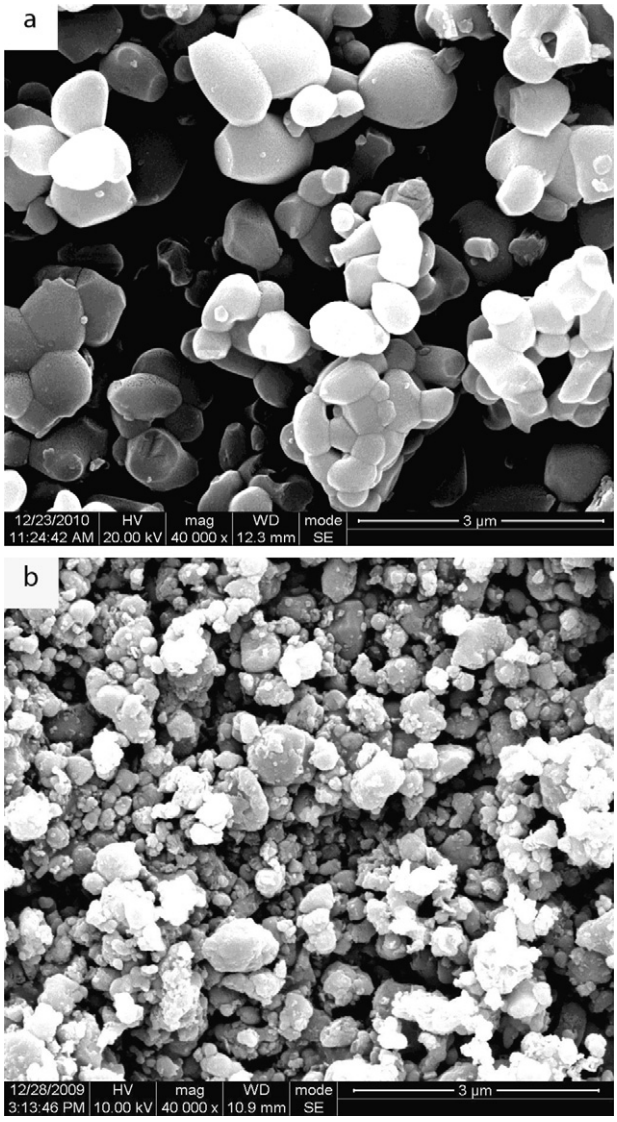

Fig. 3. SEM images of bare $LiFePO_4$ and $LiFePO_4$/C: (a) bare $LiFePO_4$, (b) $LiFePO_4$/C.

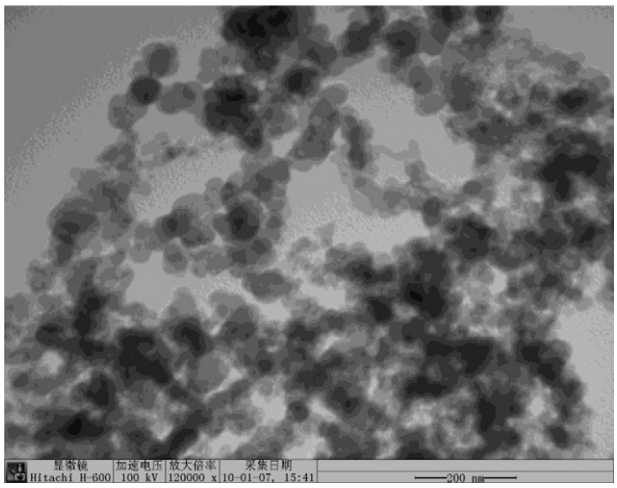

Fig. 4. TEM image of $LiFePO_4$/C composite.

To study the carbon structure, the corresponding Raman spectrum has been presented in Fig. 5. The group of peaks observed in the range of 1530–1640 cm^{-1} and 1250–1450 cm^{-1} can be assigned to the graphite band (G-band), a disorder-induced phonon mode (D-band), respectively. Higher relative intensity ratios of D/G correspond to a lower degree of order [37,38]. It is reported that olivine $LiFePO_4$ with low I_D/I_G ratios outperformed good electrochemical properties [39]. So glucose is assumed to be a good additive to improve the character of $LiFePO_4$.

To analyze the electrochemical properties of bare $LiFePO_4$ and $LiFePO_4$/C cathode material, the cyclic voltammograms of the samples were measured, as shown in Fig. 6. The anodic and cathodic peaks correspond to the two-phase charge–discharge reaction of the Fe^{2+}/Fe^{3+} redox couple. It can be observed that all the samples exhibited one oxidation peak and one reduction peak for every cycle, which indicates that only one redox reaction proceeds during the insertion and extraction of Li ions. From Fig. 6(b), it can be observed that with increasing cycle number, the anodic and cathodic peak intensities increase gradually, and the peak widths become narrower. However, for the sample $LiFePO_4$, the results are contrary. As can be seen from Fig. 6(a), as cycle number increases, the anodic and cathodic peak intensities decrease quickly, and the peak widths become wider. These different features between the two samples clearly demonstrate that carbon coating can greatly

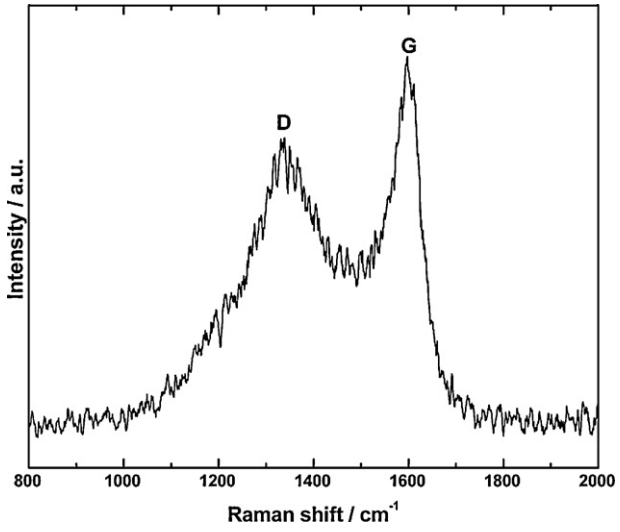

Fig. 5. The Raman spectroscopy of $LiFePO_4$/C composite.

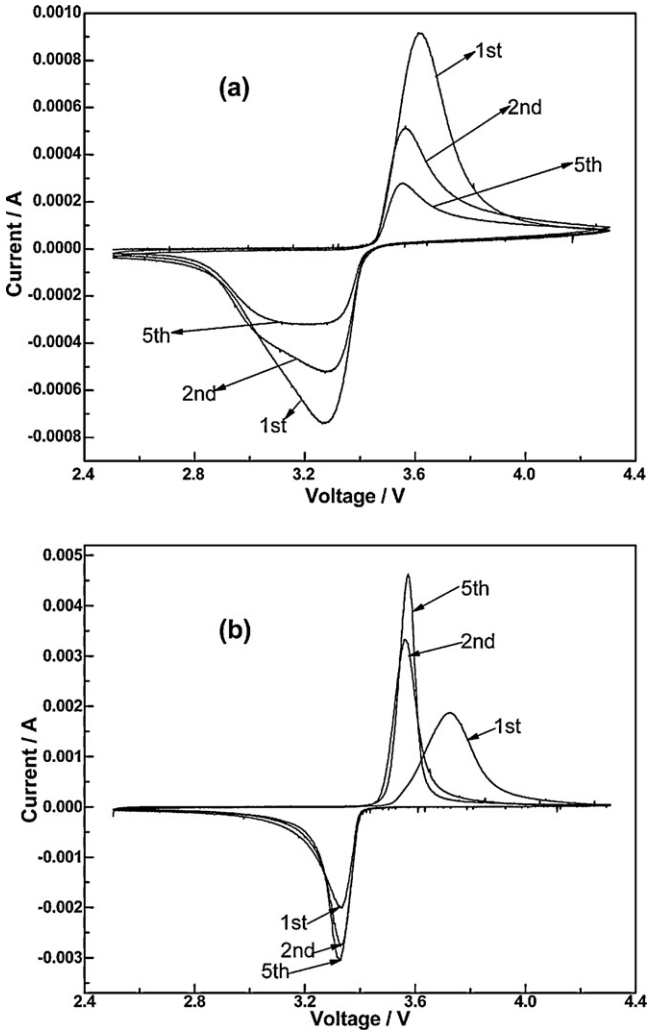

Fig. 6. Cycle CVs of bare $LiFePO_4$ and $LiFePO_4$/C at a scan rate of 0.1 mV s^{-1}: (a) bare $LiFePO_4$, (b) $LiFePO_4$/C.

improve reversible performance for the insertion and extraction of Li ion, resulting in better dynamic behaviors. This is because pyrolytic carbon can reduce the particle size of the sample, shortens the distance of the transport passage, and increases the conductivity of the sample. Therefore, the sample $LiFePO_4$/C exhibits excellent reversible performance.

The initial charge/discharge curves of $LiFePO_4$ and $LiFePO_4$/C at a rate of 0.2 C are illustrated in Fig. 7. As shown in Fig. 7, the discharge capacities of the $LiFePO_4$ and $LiFePO_4$/C are 158 and 119 mA h g^{-1}, respectively. The higher discharge capacity for sample $LiFePO_4$/C can be explained in terms of particle size, as reported previously [40,41], because the charge–discharge process is controlled by lithium transport across the $LiFePO_4$|$LiFePO_4$ interface. Consequently, the particle size is one of the critical factors in determining the electrochemical performance of $LiFePO_4$ [42–44]. On the other hand, sample $LiFePO_4$/C has carbon coating around the particles, which can also improve its electrochemical performance.

The cycle performance of bare $LiFePO_4$ and $LiFePO_4$/C is shown in Fig. 8. It can be seen that the discharge capacity of $LiFePO_4$/C gradually increases with increasing cycling number, but the discharge capacities of $LiFePO_4$ quickly decrease. The capacity retentions are 100.2% and 57.2% for samples $LiFePO_4$/C and $LiFePO_4$, respectively, after 5 cycles. The differences can be attributed to the particle size, impurities, and carbon coating.

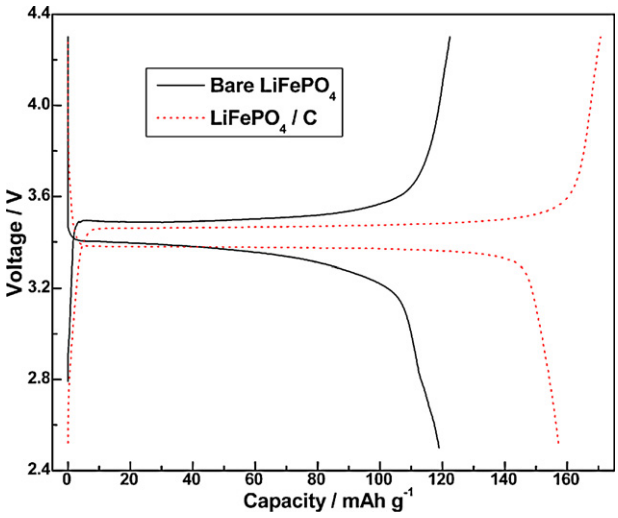

Fig. 7. Initial charge/discharge curves of $LiFePO_4$ and $LiFePO_4$/C at a rate of 0.2 C.

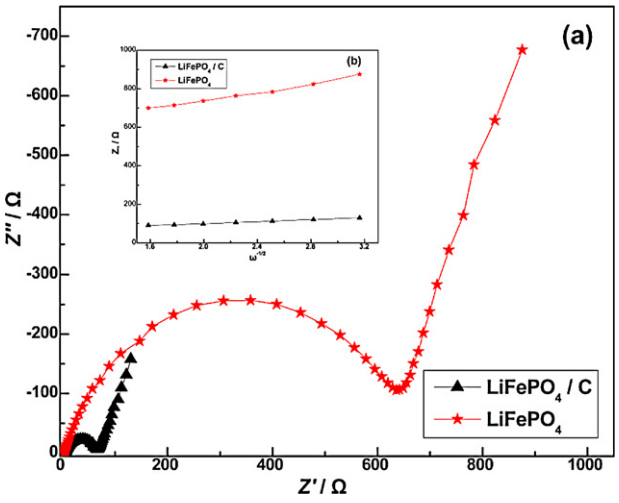

Fig. 9. (a) Electrochemical impedance spectra of bare $LiFePO_4$ and $LiFePO_4$/C. (b) The relationship plot between Z_{re} and $\omega^{-1/2}$ at low-frequency region.

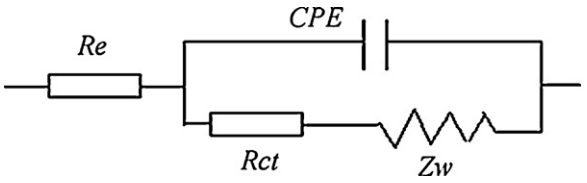

Fig. 10. Equivalent circuit used for fitting the experimental EIS data.

In order to understand the influence of carbon coating on the materials in detail, electrochemical impedance spectra measurements were carried out in a fresh coin cell, as shown in Fig. 9(a). An intercept at the Z' axis in high frequency corresponded to the ohmic resistance (R_e), which represented the resistance of the electrolyte. The semicircle in the middle frequency range indicated the charge transfer resistance (R_{ct}). The inclined line in the low frequency represented the Warburg impedance (Z_w), which was associated with lithium-ion diffusion in the $LiFePO_4$ particles. A simplified equivalent circuit model (Fig. 10) was constructed to analyze the impedance spectra. A constant phase element CPE was placed to represent the double layer capacitance and passivation film capacitance.

The lithium-ion diffusion coefficient could be calculated using the following equation [45]:

$$D = \frac{R^2T^2}{2A^2n^4F^4C^2\sigma^2} \quad (1)$$

Herein, R is the gas constant, T is the absolute temperature, A is the surface area of the cathode, n is the number of electrons per molecule during oxidization, F is the Faraday constant, C is the concentration of lithium-ion (7.69×10^{-3} mol cm^{-3}), and σ is the Warburg factor which is associated with Z_{re}.

$$Z_{re} = R_e + R_{ct} + \sigma\omega^{-1/2} \quad (2)$$

where ω is the frequency. Fig. 9(b) shows the relationship plot between Z_{re} and reciprocal square root of the angular frequency ($\omega^{-1/2}$) at low-frequency region. All the parameters obtained and calculated from EIS are shown in Table 3. It can be seen that the exchange current density ($i = RT/nFR_{ct}$) [46] of the $LiFePO_4$/C composite is higher than that bare $LiFePO_4$. Furthermore, it is obvious that the R_{ct} drastically decreases and lithium-ion diffusion coefficient increases for $LiFePO_4$/C. The reasons can be explained in terms of particle size and carbon coating, as reported previously [44,47,48], because under the same conditions, small particle can shorten the distance of the transport passage, and carbon coating can increase the conductivity of the sample and reduce the polarization on interface which may be useful for the lithium-ion diffusion. Moreover, from Fig. 3 it can be observed that there is considerable nano-sized microstructure on the surface of the sample

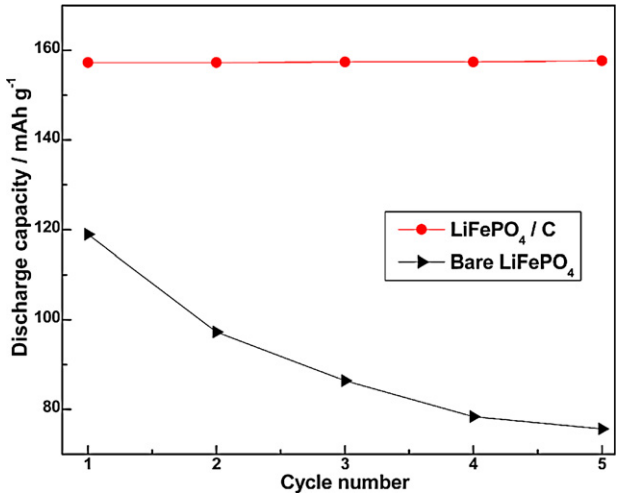

Fig. 8. Cycling performances of bare $LiFePO_4$ and $LiFePO_4$/C at a rate of 0.2 C.

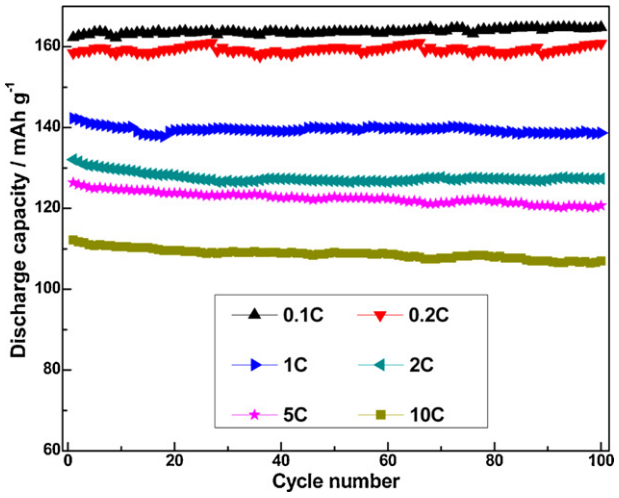

Fig. 11. Cycling performances of $LiFePO_4$/C at various discharge rates.

Table 3
The impedance parameters of the $LiFePO_4$ and $LiFePO_4$/C cells.

Sample ID	R_e (Ω)	R_{ct} (Ω)	σ (Ω cm $s^{-1/2}$)	D (cm^2 s^{-1})	i (mA cm^{-2})
$LiFePO_4$	2.89	645	120.2	1.52E−14	3.98E−05
$LiFePO_4$/C	2.71	67	25.1	3.49E−13	3.83E−04

$LiFePO_4$/C, however, sample LiFePO4 shows a glossy surface. Nano-sized microstructure on the surface may provide a lot of transport passage for lithium-ion, which also may increase the lithium-ion diffusion.

Fig. 11 presents the cycle performance of sample $LiFePO_4$/C at various discharge rates ranging from 0.1 C to 10 C. Although the discharge capacities decrease from 162 mA h g^{-1} to 112 mA h g^{-1} with the increase of discharge rates from 0.1 C to 10 C, the sample presents excellent capacity retention at different rates. The capacity retentions are 101.5%, 97.4%, 95.5%, 95.3% at rates of 0.1 C, 1 C, 5 C, 10 C, respectively, after 100 cycles. The results show that sample $LiFePO_4$/C has good rate performance and cycling stability.

4. Conclusions

Olivine $LiFePO_4$ and $LiFePO_4$/C were successfully prepared by a simple solid-state reaction using $FePO_4 \cdot 2H_2O$, lithium oxalate and glucose (bare $LiFePO_4$ without adding glucose) as raw materials. This method is a simple, high productivity and environmentally friendly synthetic route that can be applied in industrial production. The carbon coating has significant effects on the physical and electrochemical properties of the material. The results show that $LiFePO_4$/C showed the best electrochemical performance than bare $LiFePO_4$. It exhibited initial discharge capacities of 162, 142 and 112 mA h g^{-1} at rates of 0.1, 1 and 10 C, respectively, and shows excellent cycling stability.

Acknowledgements

We gratefully acknowledge the support of the National High-Tech Research & Development Program of China (863 program, No. 2009AA03Z231) and Chengdu Zhongke Laifang Energy and Technology Co. Ltd.

References

[1] D.D. MacNeil, Z.H. Lu, Z.H. Chen, J.R. Dahn, J. Power Sources 108 (2002) 8–14.
[2] M. Takahashi, S.I. Tobishima, K. Takei, Y. Sakurai, Solid State Ionics 148 (2002) 283–289.
[3] A.K. Padhi, K.S. Nanjundaswamy, J.B. Goodenough, J. Electrochem. Soc. 144 (1997) 1188–1194.
[4] R. Dominko, M. Bele, J.M. Goupil, M. Gaberscek, D. Hanzel, I. Arcon, J. Jamnik, Chem. Mater. 19 (2007) 2960–2969.
[5] B.L. Ellis, W.R.M. Makahnouk, Y. Makimura, K. Toghill, L.F. Nazar, Nat. Mater. 6 (2007) 749–753.
[6] H.-M. Xie, R.S. Wang, J.R. Ying, L.Y. Zhang, A.F. Jalbout, H.Y. Yu, G.L. Yang, X.M. Pan, Z.M. Su, Adv. Mater. 18 (2006) 2609–2913.
[7] S. Yang, Y. Song, P.Y. Zavalij, M.S. Whittingham, Electrochem. Commun. 4 (2002) 239–246.
[8] A. Yamada, M. Hosoya, S.-C. Chung, Y. Kudo, K. Hinokuma, K.Y. Liu, Y. Nishi, J. Power Sources 119–121 (2003) 232–238.
[9] R. Dominko, M. Bele, M. Gaberscek, M. Remskar, D. Hanzel, J.M. Goupil, S. Pejovnik, J. Jamnik, J. Power Sources 153 (2006) 274–280.
[10] Y.G. Wang, Y.R. Wang, E. Hosono, K.X. Wang, H.S. Zhou, Angew. Chem. Int. Ed. 47 (2008) 7461–7465.
[11] D.Y.W. Yu, C. Fietzek, W. Weydanz, K. Donoue, T. Inoue, H. Kurokawa, S. Fujitani, J. Electrochem. Soc. 154 (2007) A253–A257.
[12] L.Q. Sun, R.H. Gui, A.F. Jalbout, M.J. Li, X.M. Pan, R.S. Wang, H.M. Xie, J. Power Sources 189 (2009) 522–526.
[13] M. Konarova, I. Taniguchi, J. Power Sources 195 (2010) 3661–3667.
[14] Y. Lin, M.X. Gao, D. Zhu, Y.F. Liu, H.G. Pan, J. Power Sources 184 (2008) 444–448.
[15] P.S. Herle, B. Ellis, N. Coombs, L.F. Nazar, Nat. Mater. 3 (2004) 147–152.
[16] N. Meethong, Y.H. Kao, S.A. Speakman, Y.M. Chiang, Adv. Funct. Mater. 19 (2009) 1060–1070.
[17] A. Yamada, Y. Kudo, K.Y. Liu, J. Electrochem. Soc. 148 (2001) A1153–A1158.
[18] F. Gao, Z.Y. Tang, J.J. Xue, Electrochim. Acta 53 (2007) 1939–1944.
[19] J.C. Zheng, X.H. Li, Z.X. Wang, H.J. Guo, S. Zhou, J. Power Sources 184 (2008) 574–577.
[20] H. Chen, S.Z. Wang, Mater. Lett. 63 (2009) 1668–1670.
[21] C.Y. Lai, Q.J. Xu, H.H. Ge, G.D. Zhou, J.Y. Xie, Solid State Ionics 179 (2008) 1736–1739.
[22] H.-C. Kang, D.-K. Jun, B. Jin, E.M. Jin, K.-H. Park, H.-B. Gu, K.-W. Kim, J. Power Sources 179 (2008) 340–346.
[23] H. Liu, Y. Feng, Z.-H. Wang, K. Wang, J.-Y. Xie, Powder Technol. 184 (2008) 313–317.
[24] J.-K. Kim, J.-W. Choi, G.-S. Chauhan, J.-H. Ahn, G.-C. Hwang, J.-B. Choi, H.-J. Ahn, Electrochim. Acta 53 (2008) 8258–8264.
[25] J.F. Ni, H.H. Zhou, J.T. Chen, X.X. Zhang, Mater. Lett. 61 (2007) 1260–1264.
[26] G. Arnold, J. Garche, R. Hemmer, S. Strobele, C. Vogler, M. Wohlfahrt-Mehrens, J. Power Sources 119–121 (2003) 247–251.
[27] S.F. Yang, P.Y. Zavalij, M. Whittingham, Electrochem. Commun. 3 (2001) 505–508.
[28] G. Meligrana, C. Gerbaldi, A. Tuel, S. Bodoardo, N. Penazzi, J. Power Sources 160 (2006) 516–522.
[29] M. Higuchi, K. katayama, Y. Azuma, M. Yukawa, M. Suhara, J. Power Sources 119–121 (2003) 258–261.
[30] H.C. Shin, W.I. Cho, H. Jang, Electrochim. Acta 52 (2006) 1472–1476.
[31] J.-K. Kim, G. Cheruvally, J.-W. Choi, J.-U. Kim, J.-H. Ahn, G.-B. Cho, K.-W. Kim, H.-J. Ahn, J. Power Sources 166 (2007) 211–218.
[32] S. Franger, C. Benoit, C. Bourbon, F. Le Cras, J. Phys. Chem. Solids 67 (2006) 1338–1342.
[33] J.-K. Kim, J.-W. Choi, G. Cheruvally, J.-U. Kim, J.-H. Ahn, G.-B. Cho, K.-W. Kim, H.-J. Ahn, Mater. Lett. 61 (2007) 3822–3825.
[34] C.W. Kim, J.S. Park, K.S. Lee, J. Power Sources 163 (2006) 144–150.
[35] H.C. Shin, W.I. Cho, H. Jang, J. Power Sources 159 (2006) 1383–1388.
[36] T.H. Teng, M.R. Yang, S.H. Wu, Y.P. Chiang, Solid State Commun. 142 (2007) 389–392.
[37] H. Hiura, T.W. Ebbesen, K. Tanigaki, H. Takahashi, Chem. Phys. Lett. 202 (1993) 509–512.
[38] M.S. Bhuvaneswari, N.N. Bramnik, D. Ensling, H. Ehrenberg, W. Jaegermann, J. Power Sources 180 (2008) 553–560.
[39] M.M. Doeff, J.D. Wilcox, R. Kostecki, G. Lau, J. Power Sources 163 (2006) 180–184.
[40] Z. Chen, J.R. Dahn, J. Electrochem. Soc. 149 (2002) A1184–A1189.
[41] X.K. Zhi, G.C. Liang, L. Wang, X.Q. Qu, J.P. Zhang, J.Y. Cui, J. Power Sources 189 (2009) 779–782.
[42] M. Kunduraci, G.G. Amatucci, Electrochim. Acta 53 (2008) 4193–4199.
[43] C.-H. Lu, S.-W. Lin, J. Power Sources 97–98 (2001) 458–460.
[44] J.L. Li, C. Daniel, D. Wood, J. Power Sources 196 (2011) 2452–2460.
[45] B. Jin, E.M. Jin, K.-H. Park, H.-B. Gu, Electrochem. Commun. 10 (2008) 1537–1540.
[46] Y. Atef, K.R. Shenouda, Murali, J. Power Sources 176 (2008) 332–339.
[47] S.J. Kwon, C.W. Kim, W.T. Jeong, K.S. Lee, J. Power Sources 137 (2004) 93–99.
[48] H. Huang, S.C. Yin, L.F. Nazar, Electrochem. Solid-State Lett. 4 (2001) A170–A172.